

Towards a Comprehensive Benchmark for Pathological Lymph Node Metastasis in Breast Cancer Sections

Xitong Ling^{1,†}, Yuanyuan Lei^{2,†}, Jiawen Li^{1,†}, Junru Cheng³, Wenting Huang², Tian Guan¹, Jian Guan^{2,*}, and Yonghong He^{1,*}

¹Shenzhen International Graduate School, Tsinghua University, Shenzhen, 518071, China

²National Cancer Center/National Clinical Research Center for Cancer/Cancer Hospital & Shenzhen Hospital, Chinese Academy of Medical Sciences and Peking Union Medical College, Shenzhen, 518116, China

³Research Institute of Tsinghua, Guangzhou, 508157, China

*corresponding author(s): Yonghong He (heyh@sz.tsinghua.edu.cn), Jian Guan (graceguan9@hotmail.com)

†these authors contributed equally to this work

ABSTRACT

Advances in optical microscopy scanning have significantly contributed to computational pathology (CPath) by converting traditional histopathological slides into whole slide images (WSIs). This development enables comprehensive digital reviews by pathologists and accelerates AI-driven diagnostic support for WSI analysis. Recent advances in foundational pathology models have increased the need for benchmarking tasks. The Camelyon series^{1,2} is one of the most widely used open-source datasets in computational pathology. However, the quality, accessibility, and clinical relevance of the labels have not been comprehensively evaluated. In this study, we reprocessed 1,399 WSIs and labels from the Camelyon-16¹ and Camelyon-17² datasets, removing low-quality slides, correcting erroneous labels, and providing expert pixel annotations for tumor regions in the previously unreleased test set. Based on the sizes of re-annotated tumor regions, we upgraded the binary cancer screening task to a four-class task: negative, micro-metastasis, macro-metastasis, and Isolated Tumor Cells (ITC). We reevaluated pre-trained pathology feature extractors and multiple instance learning (MIL) methods using the cleaned dataset, providing a benchmark that advances AI development in histopathology.

Background & Summary

The efficient utilization of digital pathology and computational resources has led to the rapid rise of AI-based computational pathology^{3,4}. In recent years, general foundational models for pathology, pre-trained on large-scale data, have garnered significant attention⁵⁻⁹. These models have demonstrated strong feature extraction capabilities for pathological images, as evidenced by evaluations across a series of whole-slide image-level downstream tasks¹⁰⁻¹². For example, CTransPath⁸ uses a Semantically-Relevant Contrastive Learning (SRCL) framework to pre-train a CNN-Transformer hybrid feature extractor on 150 million patches, with its effectiveness validated across five downstream tasks. UNI⁶ employed the self-supervised DINO-v2¹³ method to train a robust general pathology visual encoder on one billion patches from approximately 100,000 whole slide images (WSIs). Gigapath⁷ utilized 1.3 billion patches to train a LongNet¹⁴ architecture-based visual encoder for slide-level representation learning. These pathology-pre-trained models have demonstrated superior performance in downstream tasks including tumor classification, survival analysis, and lesion segmentation. PLIP⁵, pre-trained on approximately 200,000 pathology image-text pairs collected from medical Twitter, developed a multimodal pathology foundational model using contrastive learning¹⁵, capable of both image and text comprehension. CONCH⁹ employs CoCa¹⁶ for self-supervised pre-training on 1.17 million image-caption pairs and has been extensively evaluated across 14 downstream benchmarks, demonstrating its outstanding performance.

Acquiring finely annotated large-scale pathology image datasets remains challenging due to the extremely high resolution of pathology images and the specialized expertise required for annotations. Nonetheless, the continued development of foundational models and downstream tasks in computational pathology makes high-quality pathology image datasets increasingly essential.

The Camelyon series^{1,2} (<http://gigadb.org/dataset/100439>), a publicly available pathology dataset focused on detecting breast cancer lymph node metastasis, is widely used for evaluating multiple instance Learning (MIL) methods. However, as shown in Figure 1, some images in the Camelyon series are of poor quality, exhibit treatment-related artifacts, and contain errors in slide-level labeling. The Camelyon-16¹ dataset includes only tumor and negative labels, making it incompatible with

Camelyon-17² labels. Many pixel-level annotations are inaccurate, and some slides lack pixel-level annotations entirely. These issues hinder the accurate evaluation of deep learning methods in downstream pathology tasks.

In this paper, we filtered out and removed slides from the Camelyon dataset that were blurred, poorly stained, exhibited treatment-related artifacts, or were ambiguous in terms of positivity. Additionally, we expanded the binary classification labels in Camelyon-16¹ to a four-class system to facilitate the merging of Camelyon-16 and Camelyon-17² datasets. Finally, we corrected the pixel-level annotations in the Camelyon dataset and added pixel-level annotations to positive slides that previously lacked them. Using the corrected dataset, we reevaluated 12 mainstream MIL methods, including ABMIL¹⁷, TransMIL¹⁸ and CIAM¹⁹, etc. on two natural image pre-trained feature encoders, ResNet-50²⁰ and VIT-S¹⁷, as well as four pathology-specific pre-trained feature encoders, PILP⁵, CONCH⁹, UNI⁶ and Gigapath⁷.

Methods

Dataset Overview

The official Camelyon-16¹ dataset contains 399 WSIs, split into 270 for training and 129 for testing. The training set includes 111 tumor slides and 259 negative slides, while the test set includes 49 tumor slides and 80 negative slides. The official Camelyon-17² dataset consists of 1000 WSIs, evenly divided into 500 for training and 500 for testing. The training set consists of 318 negative slides, 59 micro-metastasis slides, 87 macro-metastasis slides, and 36 Isolated Tumor Cells (ITC) slides. The test set labels are not publicly available. After data cleaning by professional pathologists, the Camelyon-16 dataset consists of 386 WSIs: 238 negative, 71 micro-metastasis, 69 macro-metastasis, and 8 ITC WSIs. The Camelyon-17 dataset consists of 964 WSIs: 633 negative, 103 micro-metastasis, 182 macro-metastasis, and 46 ITC WSIs. We combined the updated Camelyon-16 and Camelyon-17 datasets to form the Camelyon⁺ dataset. It consists of 1,350 WSIs: 871 negative, 174 micro-metastasis, 251 macro-metastasis, and 54 ITC WSIs.

Exclusion Criteria

We excluded certain WSIs based on the following criteria: focal blurriness, poor staining quality, difficulty distinguishing positive foci, and the presence of treatment-related artifacts. Of the 49 slides we remove, 26 show therapeutic response, 3 have staining issues, 12 exhibit focal blurring, 4 are of poor quality, and 4 contain suspicious cancerous regions. The presence of treatment response may interfere with model construction. In pathology, tumor treatment response refers to the histological changes in tumors following treatments such as surgery, chemotherapy, radiotherapy, targeted therapy, or immunotherapy, and the corresponding reaction to these treatments. Pathological analysis can assess histological indicators such as tumor cell necrosis, proliferation, and apoptosis, thereby evaluating treatment efficacy. Two typical treatment responses are tissue necrosis and fibrosis. Necrosis refers to areas of dead tissue formed after tumor cells die following treatment. Fibrosis refers to the scar tissue formed as a result of the tumor's self-repair after damage. Necrotic and fibrotic areas can affect the feature representation of tumor regions in computational pathology, thereby impacting the performance of downstream tasks.

Data Records

The Camelyon⁺ dataset is available via ScienceDB: (<https://doi.org/10.57760/sciencedb.16442>). The original WSI data can be downloaded from the official websites of Camelyon16¹ and Camelyon-17², so it has not been uploaded to the database. Slide-level labels are recorded in XLSX files. We provide the classification labels of the merged Camelyon⁺ dataset, which combines corrected versions of Camelyon-16 and Camelyon-17. The dataset includes four classification labels (negative, micro, macro, ITC) and two classification labels (negative, tumor), facilitating various downstream tasks. Since the original training dataset from Camelyon-16 is named using "tumor," "normal," and ID, we have renamed it to prevent pathologists correcting the data from forming prior judgments. The correspondence with the original naming will also be recorded and made public using a XLSX file. For positive WSIs, pixel-level annotations are provided in XML format. In order to facilitate future comparative experiments of multiple feature extractors on the Camelyon⁺ dataset, we also release the feature files extracted at 20X magnification using ResNet-50²⁰, VIT-S²¹, PLIP⁵, CONCH⁹, UNI⁶, and Gigapath⁷. The feature files are stored in PT format, which can be easily processed using the PyTorch library. Detailed dataset information and download links are available at: (<https://github.com/lingxitong/CAMELYON-PLUS-BENCHMARK>).

Technical Validation

Methodology

The objective of our designed benchmark is to utilize slide-level labels to predict metastasis types. The commonly used approach is to adopt a deep learning strategy based on MIL, which has been recognized in recent studies for its strong capability to represent slide-level features.²²⁻²⁶ MIL is a weakly supervised approach where a single WSI is treated as a bag, and each

patch within the WSI is considered an instance. If any instance is cancerous, the entire WSI is labeled as cancerous, while a WSI is classified as normal only if all instances are normal.

With the advancement of deep neural networks, embedding-based MIL has become the dominant approach for WSI analysis. In embedding-based MIL, a pre-trained feature extractor first extracts features from the WSI, followed by an aggregator that pools the features for downstream classification tasks. Mean-MIL and Max-MIL aggregate features using mean pooling and max pooling, respectively, though the pooling mechanism inevitably results in information loss. ABMIL¹⁷ introduces the attention mechanism into MIL, dynamically assigning weights to each instance based on attention scores. CLAM¹⁹ further enhances this by incorporating instance-level clustering mechanisms to introduce domain knowledge, providing additional supervision alongside attention-based weight assignments. TransMIL¹⁸ leverages self-attention within the MIL aggregator to capture relationships between different instances, thereby improving global modeling capabilities. AMD-MIL²⁷ introduces an agent mechanism into the MIL aggregator and employs threshold filtering for feature selection, improving MIL performance. DSMIL²⁸ models instance relationships directly using a dual-stream architecture and a trainable distance measurement module. DTFD²⁹ addresses the issue of limited WSIs by creating pseudo-bags. WiKG³⁰ treats WSIs as knowledge graphs, dynamically constructing neighboring nodes and directed edges based on relationships between instances, and then updates the head node using knowledge-aware attention. FR-MIL³¹ introduces a distribution re-calibration approach that adjusts the feature distribution of a WSI bag (instances) based on the statistics of the max-instance (key) feature.

Data Preprocessing

For all datasets, we crop non-overlapping 256×256 patches at $20\times$ magnification. We then use six feature extractors ResNet-50²⁰, ViT-S²¹, PLIP⁵, CONCH⁹, UNI⁶, and Gigapath⁷ to extract features from the WSIs. Subsequently, we conduct two sets of experiments. The first set is a comparative experiment on the Camelyon-17² dataset before and after label correction. The Camelyon-17-Origin dataset follows the official split, with 500 WSIs for training and 500 WSIs for testing. The Camelyon-17-Refine dataset also maintains the official split but excludes slides that fall under exclusion criteria. The Camelyon-17-Refine training set contains 492 slides, while the test set includes 472 slides. This comparative experiment evaluates the impact of dataset quality on MIL models. Since the original version of Camelyon-16¹ does not have four-class labels, we do not perform similar experiments on it. The next set is the benchmark experiments on Camelyon⁺, we evaluate using five-fold cross-validation, with each fold employing stratified sampling to maintain a fixed proportion of different classes. Since each patient has multiple slides in the Camelyon-17 dataset, in order to prevent data leakage, we ensure that slides of the same label of the same patient do not appear in the training set and the validation set at the same time.

Camelyon-17 Comparative Experiment

In the comparative experiments before and after correction on the Camelyon-17² dataset, we primarily evaluated three pathology pre-trained feature extractors: PLIP⁵, UNI⁶, and Gigapath⁷. The learning rate was set to $2e-4$, using the Adam optimizer with a weight decay of $1e-5$. We repeated the experiments with random seeds of 2023, 2024, and 2025, and reported the mean and standard deviation of the evaluation metrics as shown in Table 1 and Table 2. All experiments were conducted on a workstation equipped with 4 NVIDIA RTX 3090 GPUs. Due to the significant class imbalance in the Camelyon-17 four-class dataset, our analysis concentrated on two key evaluation metrics: AUC and F1-score. Figure 3 presents a visualization of these metrics for a single MIL model across different feature extractors, using bar charts for both the Camelyon-17-Origin and Camelyon-17-Refine datasets. This visualization effectively illustrates how these metrics vary as the dataset undergoes refinement. Our results indicate that both AUC and F1-score exhibited notable changes following the dataset's adjustment. Figure 4 further visualizes the F1-score, AUC, and their combined values, highlighting the top three models to assess the impact of dataset refinement on the performance ranking of the models. While the overall model rankings shifted to some extent after the dataset refinement, the CLAM-MB¹⁹ model consistently maintained its top-ranked position, indicating its robustness. In summary, dataset refinement enhanced the accuracy of model evaluation metrics and improved the fairness of model rankings, establishing a more solid foundation for future research.

Camelyon⁺ Benchmark Experiment

In the Benchmark Experiment on Camelyon⁺, we maintained the same hyperparameter settings as in the comparative experiments on Camelyon-17². On the merged Camelyon⁺ dataset, we evaluated the MIL approach using feature extractors from two pre-trained natural image models, ResNet-50²⁰ and ViT-S²¹, and four pre-trained pathology image models, PLIP⁵, CONCH⁹, UNI⁶, and Gigapath⁷. We classify these feature extractors into three main categories: ResNet-50²⁰ and ViT-S²¹ fall under the domain of natural image pre-training; PLIP and CONCH fall under the domain of image-text contrastive learning pre-training; and UNI, and GigaPath belong to the category of pathology-specific visual pre-training. We report the mean and variance of model performance in Table 3, Table 4 and Table 5, which can serve as baselines and references for future work based on the Camelyon⁺ dataset.

As shown in Figure 5, we present a heatmap of the distribution of AUC and F1-score across different MIL models under various feature extractors. It can be observed that pathology-pretrained feature extractors significantly enhance the performance of MIL. Notably, the CONCH⁹ model, which uses a ViT-Base¹⁷ architecture with image-text contrastive learning, achieves performance comparable to the UNI⁶ and Gigapath⁷ models, which utilize ViT-Large¹⁷ and ViT-Giant¹⁷ architectures, respectively. Moreover, both UNI and Gigapath leverage larger training datasets. This suggests that image-text contrastive pretraining may hold greater potential than pure visual pretraining in the pathology domain. While the PLIP⁵ model is also pretrained using image-text contrastive learning, its performance does not match that of CONCH, likely due to its smaller dataset and the lower quality of data sourced from Twitter.

In the benchmark results, while the model demonstrates relatively strong performance in terms of accuracy and AUC, the F1-score, recall, and precision are notably low. As illustrated in Figure 6, we visualized the confusion matrices for the CLAM-MB¹⁹ and FR-MIL³¹ models. The results show that the models perform relatively well in classifying the negative, micro, and macro categories, but perform poorly in the ITC category. We used macro-averaging to calculate the F1-score, recall, and precision, and the model's poor performance on the ITC category significantly lowered the overall performance metrics. To investigate this issue further, we analyzed the model's difficulty in identifying ITC cases. One major factor is the severe class imbalance in the Camelyon⁺ dataset. As shown in Figure 2, the head class, negative, contains 871 slides, while the tail class, ITC, contains only 54 slides, resulting in an imbalance ratio of approximately 16.1. This imbalance classifies the dataset as having a moderately long-tailed distribution. Such imbalance highlights a key challenge in pathology image analysis: how to achieve balanced model performance on long-tailed datasets like Camelyon⁺, particularly since real-world pathological data naturally follow a long-tailed distribution. Furthermore, we identified a fundamental difference between the four-class classification task in Camelyon⁺ and typical cancer subtyping tasks, such as those in TCGA-NSCLC, TCGA-RCC, or BRACS. The ITC, micro, and macro categories in Camelyon⁺ are primarily distinguished by the size of metastatic regions, whereas MIL is generally better suited for binary classification tasks, such as detecting the presence or absence of cancer. This explains why models achieve high performance on binary tasks like those in Camelyon-16¹ or Camelyon-17². Consequently, Camelyon⁺ raises an important question about whether the MIL approach the most suitable paradigm for clinical classification tasks like Camelyon⁺, where categories are defined by the size of metastatic regions rather than distinct subtypes of cancer.

Evaluation metrics

In the comparative experiments on the Camelyon-17² dataset and Benchmark experiments, we used accuracy, AUC, F1-score, recall, precision, and kappa value to assess classification performance. The Kappa coefficient is a statistical measure used to evaluate the level of agreement in classification models. It is commonly employed to assess classifier performance, particularly in multi-class classification tasks. This coefficient measures how well the predicted results align with actual labels while accounting for the agreement that could occur by chance. We calculated these metrics using the macro method, while results based on the micro and weighted methods will be available at (<https://github.com/lingxitong/CAMELYON-PLUS-BENCHMARK>).

Usage Notes

The Camelyon⁺ Dataset is publicly available under the Creative Commons Zero (CC0) license. However, please note that this dataset is not intended for developing diagnosis-focused algorithms or models, and should not be used as the sole basis for clinical evaluations in classification tasks.

Code availability

The code related to dataset partitioning strategies, hyperparameter configurations, integration of MIL methods, and evaluation metric calculations will be made publicly available at: (https://github.com/lingxitong/MIL_BASELINE).

References

1. Bejnordi, B. E. *et al.* Diagnostic assessment of deep learning algorithms for detection of lymph node metastases in women with breast cancer. *Jama* **318**, 2199–2210 (2017).
2. Bandi, P. *et al.* From detection of individual metastases to classification of lymph node status at the patient level: the camelyon17 challenge. *IEEE transactions on medical imaging* **38**, 550–560 (2018).
3. Song, A. H. *et al.* Artificial intelligence for digital and computational pathology. *Nat. Rev. Bioeng.* **1**, 930–949 (2023).
4. Van der Laak, J., Litjens, G. & Ciompi, F. Deep learning in histopathology: the path to the clinic. *Nat. medicine* **27**, 775–784 (2021).

5. Huang, Z., Bianchi, F., Yuksekogonul, M., Montine, T. J. & Zou, J. A visual–language foundation model for pathology image analysis using medical twitter. *Nat. medicine* **29**, 2307–2316 (2023).
6. Chen, R. J. *et al.* Towards a general-purpose foundation model for computational pathology. *Nat. Medicine* **30**, 850–862 (2024).
7. Xu, H. *et al.* A whole-slide foundation model for digital pathology from real-world data. *Nature* 1–8 (2024).
8. Wang, X. *et al.* Transformer-based unsupervised contrastive learning for histopathological image classification. *Med. image analysis* **81**, 102559 (2022).
9. Lu, M. Y. *et al.* A visual-language foundation model for computational pathology. *Nat. Medicine* **30**, 863–874 (2024).
10. Kather, J. N. *et al.* Predicting survival from colorectal cancer histology slides using deep learning: A retrospective multicenter study. *PLoS medicine* **16**, e1002730 (2019).
11. Pataki, B. Á. *et al.* Hunccr: annotated pathological slides to enhance deep learning applications in colorectal cancer screening. *Sci. Data* **9**, 370 (2022).
12. Barbano, C. A. *et al.* Unitopatho, a labeled histopathological dataset for colorectal polyps classification and adenoma dysplasia grading. In *2021 IEEE International Conference on Image Processing (ICIP)*, 76–80 (IEEE, 2021).
13. Oquab, M. *et al.* Dinov2: Learning robust visual features without supervision. *arXiv preprint arXiv:2304.07193* (2023).
14. Ding, J. *et al.* Longnet: Scaling transformers to 1,000,000,000 tokens. *arXiv preprint arXiv:2307.02486* (2023).
15. Radford, A. *et al.* Learning transferable visual models from natural language supervision. In *International conference on machine learning*, 8748–8763 (PMLR, 2021).
16. Yu, J. *et al.* Coca: Contrastive captioners are image-text foundation models. *arXiv preprint arXiv:2205.01917* (2022).
17. Ilse, M., Tomczak, J. & Welling, M. Attention-based deep multiple instance learning. In *International conference on machine learning*, 2127–2136 (PMLR, 2018).
18. Shao, Z. *et al.* Transmil: Transformer based correlated multiple instance learning for whole slide image classification. *Adv. neural information processing systems* **34**, 2136–2147 (2021).
19. Lu, M. Y. *et al.* Data-efficient and weakly supervised computational pathology on whole-slide images. *Nat. biomedical engineering* **5**, 555–570 (2021).
20. He, K., Zhang, X., Ren, S. & Sun, J. Deep residual learning for image recognition. In *Proceedings of the IEEE conference on computer vision and pattern recognition*, 770–778 (2016).
21. Dosovitskiy, A. An image is worth 16x16 words: Transformers for image recognition at scale. *arXiv preprint arXiv:2010.11929* (2020).
22. Yan, R. *et al.* Shapley values-enabled progressive pseudo bag augmentation for whole-slide image classification. *IEEE Transactions on Med. Imaging* (2024).
23. Ouyang, M. *et al.* Mergeup-augmented semi-weakly supervised learning for wsi classification. *arXiv preprint arXiv:2408.12825* (2024).
24. Chu, H. *et al.* Retmil: Retentive multiple instance learning for histopathological whole slide image classification. In *International Conference on Medical Image Computing and Computer-Assisted Intervention*, 437–447 (Springer, 2024).
25. Qiehe, S. *et al.* Nciemil: Rethinking decoupled multiple instance learning framework for histopathological slide classification. In *Medical Imaging with Deep Learning* (2024).
26. Yang, S., Wang, Y. & Chen, H. Mambamil: Enhancing long sequence modeling with sequence reordering in computational pathology. In *International Conference on Medical Image Computing and Computer-Assisted Intervention*, 296–306 (Springer, 2024).
27. Ling, X. *et al.* Agent aggregator with mask denoise mechanism for histopathology whole slide image analysis. *arXiv preprint arXiv:2409.11664* (2024).
28. Li, B., Li, Y. & Eliceiri, K. W. Dual-stream multiple instance learning network for whole slide image classification with self-supervised contrastive learning. In *Proceedings of the IEEE/CVF conference on computer vision and pattern recognition*, 14318–14328 (2021).
29. Zhang, H. *et al.* Dtf-d-mil: Double-tier feature distillation multiple instance learning for histopathology whole slide image classification. In *Proceedings of the IEEE/CVF conference on computer vision and pattern recognition*, 18802–18812 (2022).

30. Li, J. *et al.* Dynamic graph representation with knowledge-aware attention for histopathology whole slide image analysis. In *Proceedings of the IEEE/CVF Conference on Computer Vision and Pattern Recognition*, 11323–11332 (2024).
31. Chikontwe, P. *et al.* Fr-mil: Distribution re-calibration based multiple instance learning with transformer for whole slide image classification. *IEEE Transactions on Med. Imaging* 1–1, [10.1109/TMI.2024.3446716](https://doi.org/10.1109/TMI.2024.3446716) (2024).
32. Deng, J. *et al.* Imagenet: A large-scale hierarchical image database. In *2009 IEEE conference on computer vision and pattern recognition*, 248–255 (Ieee, 2009).

Acknowledgements

This work was supported by the National Natural Science Foundation of China (NSFC) under Grant No. 82430062. We also gratefully acknowledge the support from the Shenzhen Engineering Research Centre (Grant No. XMHT20230115004) and the Shenzhen Science and Technology Innovation Commission (Grant No. KCXFZ20201221173207022). This work was also supported by the Shenzhen High-level Hospital Construction Fund. Additionally, we thank the Jilin FuyuanGuan Food Group Co., Ltd. for their collaboration.

Author contributions statement

X.L. and J.L. conceptualized the study, designed the experiments, and conducted the specific experiments. Y.L., J.C., and W.H. were responsible for dataset correction and construction. T.G., J.G., and Y.H. contributed to the manuscript writing and provided insights into the development of the manuscript structure. All authors read and approved the final version of the manuscript.

Competing interests

The authors declare no competing interests.

Figures & Tables

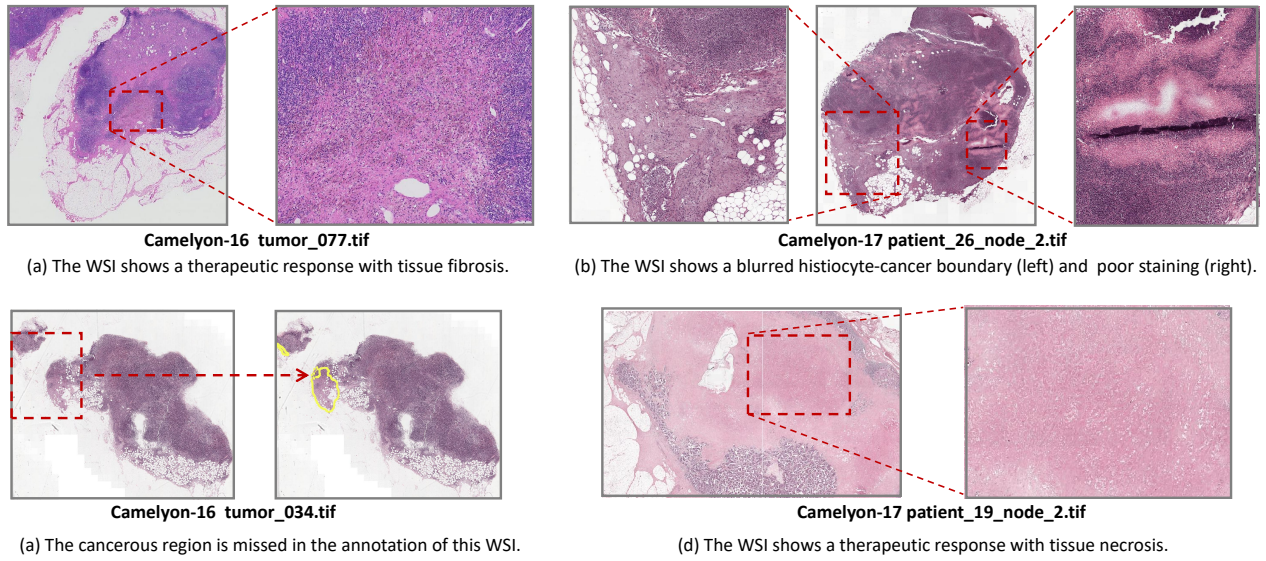


Figure 1. Issues within the Camelyon-16¹ and Camelyon-17² datasets: therapeutic response, annotation omissions, blurred boundaries, and poor staining.

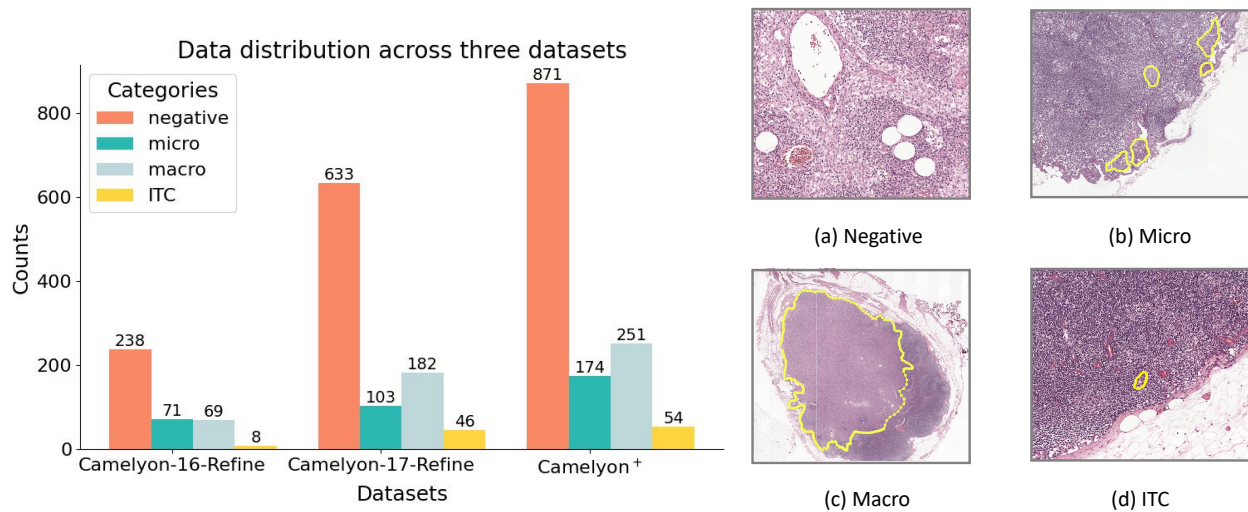


Figure 2. Revised data distribution of the Camelyon dataset and the pathological characteristics of different categories.

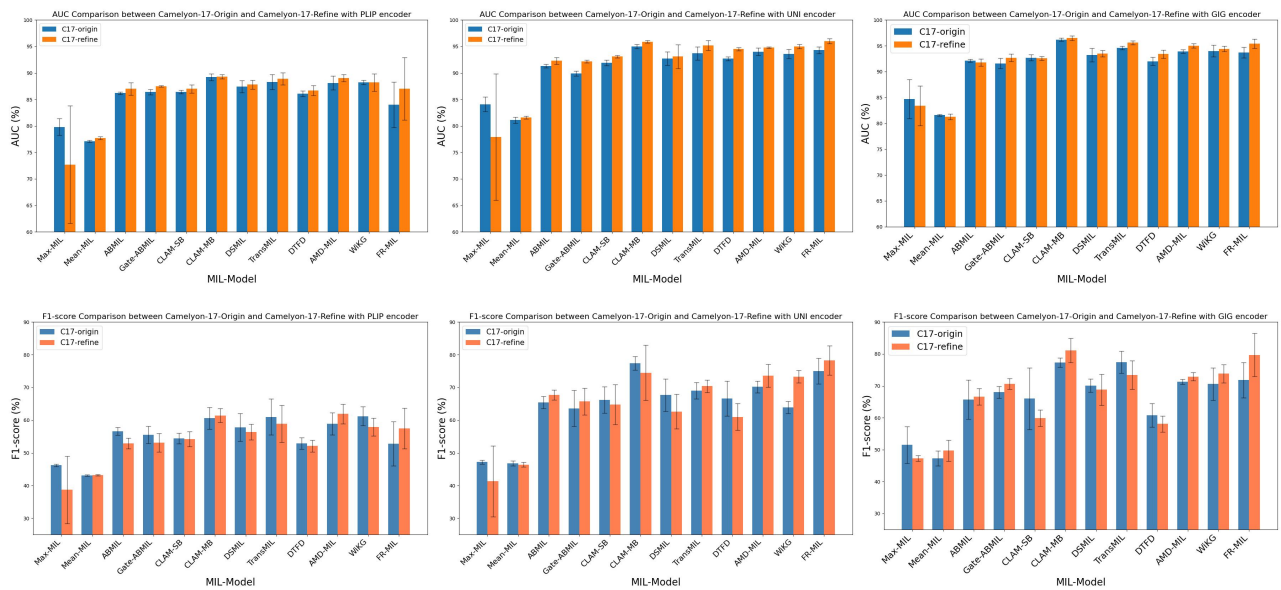


Figure 3. AUC and F1-score Comparison of Different Methods in the Camelyon-17-Origin and Camelyon-17-Refine Comparative Experiments.

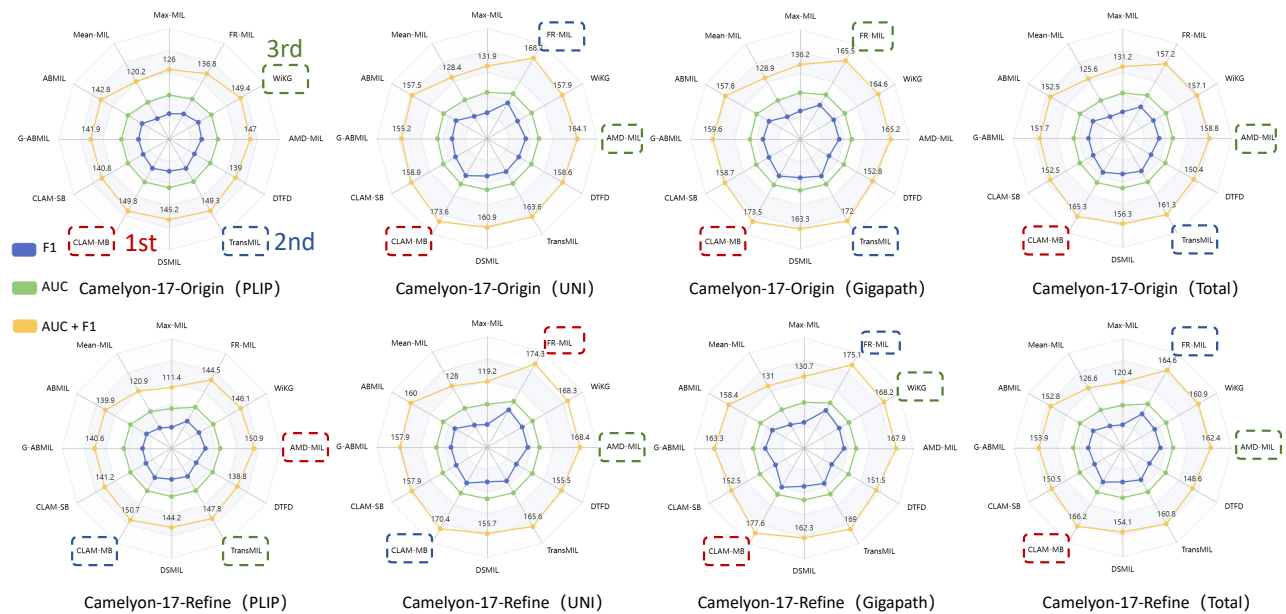


Figure 4. Model ranking radar chart based on AUC and F1-score on Camelyon-17-Origin and Camelyon-17-Refine datasets.

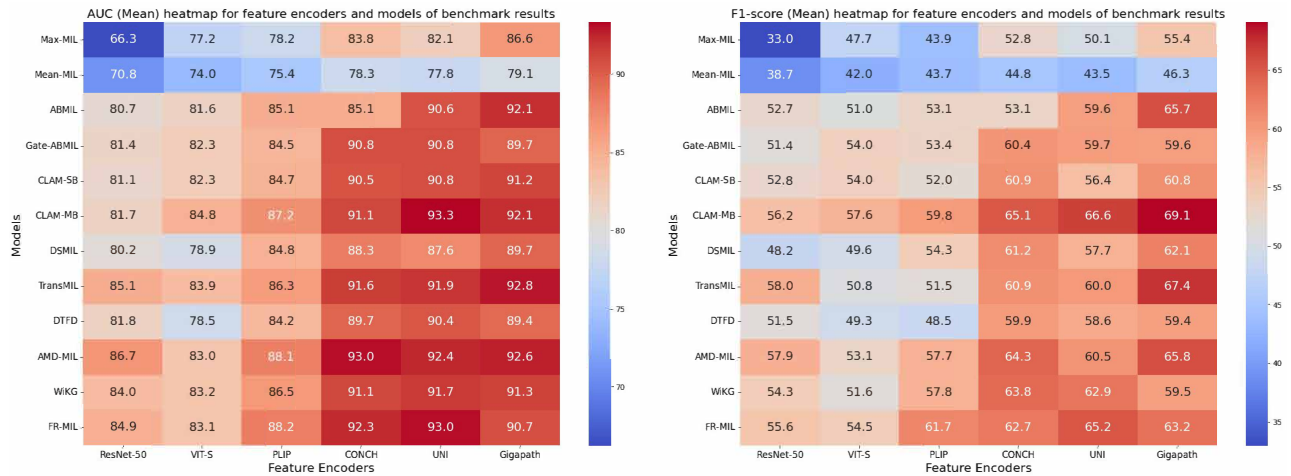


Figure 5. Distribution of AUC and F1-score in benchmark results across different feature extractors and aggregators.

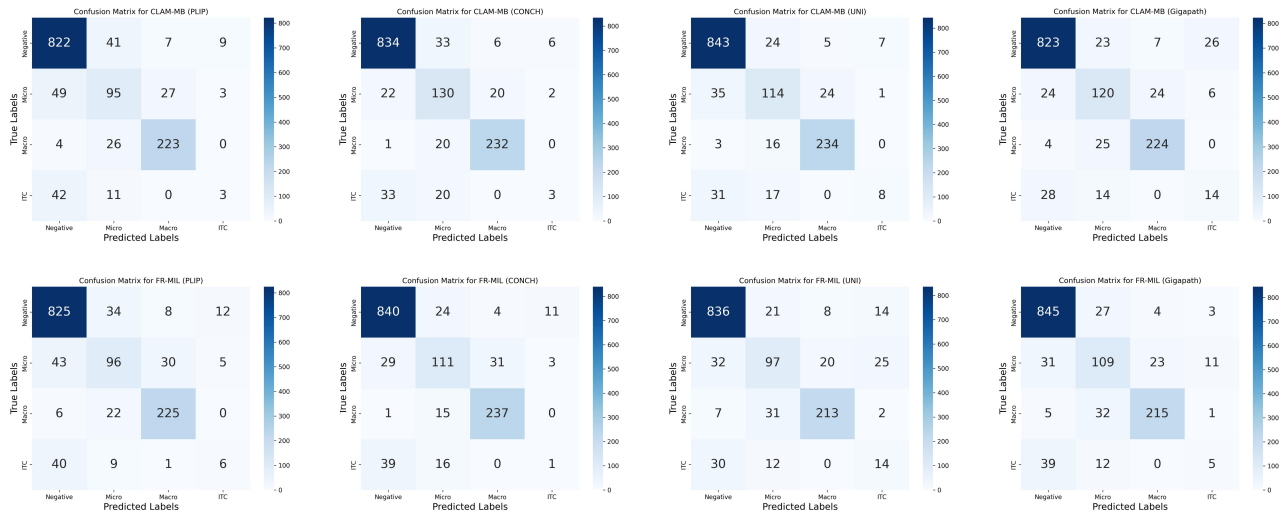


Figure 6. Confusion matrices of CLAM-MB¹⁹ and FR-MIL³¹ under the PLIP⁵, CONCH⁶, UNI⁹, and Gigapath⁷ feature encoders.

Table 1. Performance metrics of different methods on the Camelyon-17-Origin dataset.

Methods	Acc (%)	AUC (%)	F1 (%)	Recall (%)	Precision (%)	Kappa
PLIP ⁵ (WSIs pre-trained)						
Max-MIL	83.1 ± 0.90	79.8 ± 1.58	46.2 ± 0.34	45.4 ± 0.83	46.6 ± 2.35	0.69 ± 0.00
Mean-MIL	78.7 ± 0.64	77.1 ± 0.17	43.1 ± 0.25	44.5 ± 0.43	49.3 ± 1.58	0.56 ± 0.01
ABMIL ¹⁷	84.4 ± 0.72	86.2 ± 0.24	56.6 ± 1.17	54.4 ± 0.31	53.5 ± 0.45	0.77 ± 0.01
Gate-ABMIL ¹⁷	83.9 ± 1.30	86.4 ± 0.50	55.5 ± 2.66	53.8 ± 1.78	53.3 ± 0.69	0.76 ± 0.02
CLAM-SB ¹⁹	84.9 ± 0.50	86.4 ± 0.32	54.4 ± 1.63	53.2 ± 1.05	52.5 ± 0.55	0.76 ± 0.01
CLAM-MB ¹⁹	86.1 ± 0.42	89.2 ± 0.62	60.6 ± 3.30	58.4 ± 2.58	59.4 ± 5.25	0.79 ± 0.02
DSMIL ²⁸	86.1 ± 0.61	87.4 ± 1.14	57.8 ± 4.20	57.9 ± 3.57	61.2 ± 6.58	0.76 ± 0.02
TransMIL ¹⁸	85.4 ± 1.11	88.3 ± 1.42	61.0 ± 5.51	58.3 ± 4.43	56.7 ± 4.24	0.74 ± 0.06
DTFD ²⁹	85.5 ± 0.50	86.1 ± 0.55	52.9 ± 1.79	52.1 ± 2.14	52.6 ± 1.01	0.76 ± 0.01
AMD-MIL ²⁷	83.7 ± 3.18	88.1 ± 1.31	58.9 ± 3.40	56.4 ± 4.36	55.1 ± 4.74	0.73 ± 0.02
WiKG ³⁰	86.3 ± 1.22	88.2 ± 0.41	61.2 ± 2.91	59.1 ± 3.13	58.4 ± 3.04	0.78 ± 0.01
FR-MIL ³¹	82.7 ± 3.64	84.0 ± 4.32	52.8 ± 6.72	52.0 ± 5.30	52.1 ± 4.52	0.71 ± 0.07
UNI ⁶ (WSIs pre-trained)						
Max-MIL	85.3 ± 0.58	84.1 ± 1.40	47.2 ± 0.59	44.8 ± 0.75	45.0 ± 4.80	0.72 ± 0.03
Mean-MIL	76.1 ± 2.66	81.1 ± 0.55	46.8 ± 0.74	47.0 ± 1.25	48.4 ± 2.37	0.57 ± 0.03
ABMIL ¹⁷	82.4 ± 0.35	91.3 ± 0.35	65.4 ± 1.86	61.2 ± 1.35	59.7 ± 1.63	0.73 ± 0.02
Gate-ABMIL ¹⁷	80.9 ± 1.40	89.9 ± 0.44	63.6 ± 5.47	58.8 ± 4.05	56.7 ± 3.37	0.71 ± 0.02
CLAM-SB ¹⁹	81.3 ± 1.86	91.9 ± 0.53	66.2 ± 4.04	59.9 ± 2.85	58.5 ± 1.61	0.70 ± 0.04
CLAM-MB ¹⁹	85.1 ± 0.31	95.0 ± 0.41	77.4 ± 2.02	68.1 ± 1.20	64.9 ± 0.55	0.70 ± 0.02
DSMIL ²⁸	83.2 ± 0.53	92.7 ± 1.27	67.7 ± 4.95	61.8 ± 3.23	60.2 ± 2.49	0.66 ± 0.05
TransMIL ¹⁸	86.0 ± 0.35	93.7 ± 1.24	69.0 ± 2.47	64.4 ± 2.31	64.4 ± 1.92	0.77 ± 0.02
DTFD ²⁹	84.4 ± 0.60	92.7 ± 0.37	66.6 ± 5.33	61.7 ± 5.15	59.2 ± 4.56	0.77 ± 0.04
AMD-MIL ²⁷	82.5 ± 1.62	94.0 ± 0.70	70.2 ± 1.79	63.0 ± 1.60	61.1 ± 1.04	0.63 ± 0.06
WiKG ³⁰	84.6 ± 3.20	93.6 ± 0.87	63.9 ± 1.87	60.0 ± 1.72	58.4 ± 1.25	0.72 ± 0.08
FR-MIL ³¹	84.1 ± 0.70	94.3 ± 0.66	75.0 ± 3.91	66.2 ± 2.13	63.5 ± 1.28	0.71 ± 0.01
Gigapath ⁷ (WSIs pre-trained)						
Max-MIL	83.5 ± 1.81	84.7 ± 3.79	51.5 ± 5.76	49.5 ± 5.31	48.2 ± 4.85	0.74 ± 0.04
Mean-MIL	78.3 ± 1.36	81.6 ± 0.17	47.3 ± 2.31	48.7 ± 1.69	53.2 ± 3.11	0.53 ± 0.05
ABMIL ¹⁷	79.2 ± 2.43	92.1 ± 0.27	65.7 ± 6.11	58.1 ± 5.31	58.6 ± 0.99	0.68 ± 0.03
Gate-ABMIL ¹⁷	80.7 ± 1.14	91.6 ± 0.99	68.0 ± 1.85	61.9 ± 1.88	60.0 ± 1.55	0.72 ± 0.02
CLAM-SB ¹⁹	80.3 ± 4.02	92.7 ± 0.59	66.0 ± 9.69	60.1 ± 8.21	61.4 ± 4.20	0.75 ± 0.01
CLAM-MB ¹⁹	85.5 ± 0.61	96.2 ± 0.30	77.3 ± 1.45	68.3 ± 0.94	65.2 ± 0.73	0.70 ± 0.02
DSMIL ²⁸	86.2 ± 1.71	93.2 ± 1.30	70.1 ± 2.06	65.6 ± 0.86	63.6 ± 1.00	0.71 ± 0.01
TransMIL ¹⁸	84.7 ± 2.21	94.6 ± 0.36	77.4 ± 3.45	68.3 ± 3.26	64.6 ± 3.06	0.73 ± 0.04
DTFD ²⁹	81.5 ± 1.22	92.0 ± 0.80	60.8 ± 3.69	55.6 ± 3.66	54.2 ± 2.66	0.75 ± 0.07
AMD-MIL ²⁷	83.5 ± 1.03	93.9 ± 0.36	71.3 ± 0.79	64.7 ± 0.38	62.9 ± 1.31	0.74 ± 0.01
WiKG ³⁰	83.4 ± 0.72	94.0 ± 1.13	70.6 ± 5.09	64.5 ± 2.23	63.0 ± 1.46	0.74 ± 0.05
FR-MIL ³¹	83.9 ± 0.81	93.7 ± 1.02	71.8 ± 5.51	64.8 ± 3.34	62.3 ± 2.78	0.70 ± 0.04

Table 2. Performance metrics of different methods on the Camelyon-17-Refine dataset.

Methods	Acc (%)	AUC (%)	F1 (%)	Recall (%)	Precision (%)	Kappa
PLIP ⁵ (WSIs pre-trained)						
Max-MIL	77.8 ± 9.55	72.7 ± 11.09	38.7 ± 10.28	37.4 ± 10.63	41.0 ± 3.25	0.49 ± 0.32
Mean-MIL	79.8 ± 0.24	77.7 ± 0.25	43.2 ± 0.18	44.8 ± 0.22	49.2 ± 0.57	0.59 ± 0.00
ABMIL ¹⁷	81.8 ± 1.39	87.0 ± 1.18	52.9 ± 1.63	51.0 ± 1.48	51.5 ± 0.42	0.75 ± 0.02
Gate-ABMIL ¹⁷	81.9 ± 2.04	87.5 ± 0.13	53.1 ± 2.83	51.3 ± 2.61	51.7 ± 1.01	0.75 ± 0.02
CLAM-SB ¹⁹	82.8 ± 1.73	87.0 ± 0.76	54.2 ± 2.32	52.3 ± 1.95	52.0 ± 0.88	0.76 ± 0.02
CLAM-MB ¹⁹	87.2 ± 0.80	89.3 ± 0.41	61.4 ± 2.12	59.6 ± 2.69	61.2 ± 7.85	0.82 ± 0.01
DSMIL ²⁸	86.2 ± 1.32	87.8 ± 0.86	56.4 ± 2.37	56.2 ± 1.95	56.5 ± 1.79	0.76 ± 0.02
TransMIL ¹⁸	83.8 ± 1.00	88.9 ± 1.15	58.9 ± 5.70	56.9 ± 4.14	56.7 ± 2.78	0.71 ± 0.02
DTFD ²⁹	84.3 ± 1.81	86.7 ± 0.95	52.1 ± 1.79	51.2 ± 1.12	51.3 ± 0.19	0.77 ± 0.01
AMD-MIL ²⁷	86.4 ± 0.97	89.0 ± 0.67	61.9 ± 3.01	59.6 ± 3.07	58.4 ± 2.66	0.78 ± 0.03
WiKG ³⁰	87.1 ± 1.20	88.2 ± 1.64	57.9 ± 2.76	56.6 ± 2.13	55.8 ± 1.86	0.80 ± 0.03
FR-MIL ³¹	80.6 ± 1.59	87.0 ± 5.90	57.5 ± 6.19	55.3 ± 4.36	54.8 ± 3.49	0.63 ± 0.02
UNI ⁶ (WSIs pre-trained)						
Max-MIL	79.6 ± 10.07	77.9 ± 11.95	41.3 ± 10.87	39.1 ± 9.87	41.1 ± 2.10	0.55 ± 0.35
Mean-MIL	76.5 ± 2.02	81.6 ± 0.26	46.4 ± 0.70	46.8 ± 1.09	49.4 ± 0.83	0.49 ± 0.06
ABMIL ¹⁷	82.1 ± 1.60	92.3 ± 0.64	67.7 ± 1.51	61.9 ± 1.47	59.6 ± 1.29	0.72 ± 0.02
Gate-ABMIL ¹⁷	81.0 ± 0.86	92.2 ± 0.28	65.7 ± 4.13	59.7 ± 3.14	57.9 ± 2.48	0.68 ± 0.05
CLAM-SB ¹⁹	81.3 ± 1.07	93.1 ± 0.22	64.8 ± 6.08	58.5 ± 4.25	56.5 ± 3.85	0.73 ± 0.07
CLAM-MB ¹⁹	85.0 ± 0.68	95.9 ± 0.21	74.5 ± 8.42	65.6 ± 3.72	63.4 ± 3.06	0.70 ± 0.08
DSMIL ²⁸	85.9 ± 3.17	93.1 ± 2.26	62.6 ± 5.28	59.9 ± 3.16	59.0 ± 1.35	0.75 ± 0.05
TransMIL ¹⁸	88.5 ± 0.44	95.2 ± 0.93	70.4 ± 1.88	65.7 ± 1.97	66.1 ± 6.04	0.78 ± 0.06
DTFD ²⁹	82.6 ± 0.56	94.5 ± 0.31	61.0 ± 4.13	56.5 ± 4.67	56.6 ± 5.77	0.78 ± 0.01
AMD-MIL ²⁷	86.0 ± 1.12	94.8 ± 0.13	73.6 ± 3.45	68.5 ± 1.14	66.8 ± 2.55	0.78 ± 0.03
WiKG ³⁰	83.1 ± 3.56	95.0 ± 0.42	73.3 ± 1.91	64.6 ± 3.19	62.6 ± 1.50	0.68 ± 0.03
FR-MIL ³¹	85.0 ± 0.97	96.0 ± 0.46	78.3 ± 4.48	68.0 ± 1.51	65.4 ± 1.22	0.70 ± 0.09
Gigapath ⁷ (WSIs pre-trained)						
Max-MIL	83.7 ± 2.77	83.4 ± 3.83	47.3 ± 0.92	45.9 ± 0.76	44.9 ± 1.69	0.75 ± 0.03
Mean-MIL	76.1 ± 4.24	81.3 ± 0.55	49.7 ± 3.29	49.5 ± 0.91	52.1 ± 1.32	0.51 ± 0.06
ABMIL ¹⁷	81.4 ± 0.49	91.8 ± 0.70	66.6 ± 2.55	61.6 ± 2.21	59.8 ± 2.55	0.75 ± 0.03
Gate-ABMIL ¹⁷	81.4 ± 1.73	92.7 ± 0.73	70.6 ± 1.69	63.2 ± 2.80	61.1 ± 2.50	0.72 ± 0.07
CLAM-SB ¹⁹	78.7 ± 2.33	92.6 ± 0.38	59.9 ± 2.54	54.8 ± 1.68	55.2 ± 4.44	0.72 ± 0.08
CLAM-MB ¹⁹	84.4 ± 1.92	96.5 ± 0.44	81.1 ± 3.75	68.5 ± 0.39	65.6 ± 0.30	0.64 ± 0.09
DSMIL ²⁸	86.2 ± 0.85	93.5 ± 0.61	68.8 ± 4.85	65.2 ± 3.73	63.8 ± 3.42	0.75 ± 0.06
TransMIL ¹⁸	86.2 ± 0.76	95.6 ± 0.36	73.4 ± 4.51	67.9 ± 4.69	66.5 ± 4.56	0.80 ± 0.02
DTFD ²⁹	80.9 ± 1.18	93.4 ± 0.81	58.1 ± 2.52	52.7 ± 1.53	53.5 ± 1.32	0.76 ± 0.02
AMD-MIL ²⁷	84.6 ± 1.20	95.0 ± 0.41	72.9 ± 1.31	66.4 ± 1.12	64.9 ± 2.85	0.75 ± 0.07
WiKG ³⁰	83.8 ± 1.41	94.4 ± 0.52	73.8 ± 2.83	66.0 ± 2.31	63.8 ± 1.39	0.74 ± 0.04
FR-MIL ³¹	85.9 ± 0.88	95.4 ± 0.89	79.7 ± 6.78	69.2 ± 2.62	65.7 ± 1.82	0.72 ± 0.04

Table 3. Benchmark results on Camelyon⁺ dataset of the natural images pre-trained domain.

Methods	Acc (%)	AUC (%)	F1 (%)	Recall (%)	Precision (%)	Kappa
ResNet-50 ²⁰ (ImageNet pre-trained ³²)						
Max-MIL	70.3 ± 7.53	66.3 ± 11.07	33.0 ± 10.65	28.9 ± 12.06	30.8 ± 13.43	0.22 ± 0.30
Mean-MIL	73.2 ± 2.87	70.8 ± 4.14	38.7 ± 3.35	37.9 ± 2.67	41.1 ± 1.77	0.39 ± 0.08
ABMIL ¹⁷	81.1 ± 1.30	80.7 ± 3.32	52.7 ± 1.98	51.5 ± 1.86	52.8 ± 1.98	0.63 ± 0.03
Gate-ABMIL ¹⁷	80.5 ± 1.26	81.4 ± 3.05	51.4 ± 2.05	49.2 ± 3.41	51.2 ± 2.99	0.63 ± 0.03
CLAM-SB ¹⁹	80.2 ± 1.78	81.1 ± 2.93	52.8 ± 2.07	50.9 ± 2.03	51.3 ± 2.51	0.63 ± 0.02
CLAM-MB ¹⁹	83.5 ± 1.22	81.7 ± 1.89	56.2 ± 3.80	56.1 ± 2.83	57.9 ± 1.75	0.65 ± 0.03
DSMIL ²⁸	79.8 ± 1.05	80.2 ± 4.10	48.2 ± 0.70	46.9 ± 1.67	49.1 ± 4.71	0.61 ± 0.01
TransMIL ¹⁸	81.2 ± 4.49	85.1 ± 1.83	58.0 ± 3.27	56.5 ± 4.00	56.8 ± 5.46	0.63 ± 0.03
DTFD ²⁹	80.6 ± 1.94	81.8 ± 4.04	51.5 ± 2.22	49.7 ± 2.57	51.2 ± 3.36	0.63 ± 0.03
AMD-MIL ²⁷	81.1 ± 1.91	86.7 ± 3.43	57.9 ± 3.03	55.8 ± 1.81	55.8 ± 1.81	0.63 ± 0.03
WiKG ³⁰	81.3 ± 3.30	84.0 ± 3.77	54.3 ± 3.24	54.3 ± 3.60	56.2 ± 3.22	0.62 ± 0.03
FR-MIL ³¹	82.8 ± 0.87	84.9 ± 2.97	55.6 ± 2.56	56.4 ± 1.29	58.5 ± 1.63	0.63 ± 0.04
ViT-S ²¹ (ImageNet pre-trained ³²)						
Max-MIL	76.7 ± 5.30	77.2 ± 1.90	47.7 ± 1.17	45.4 ± 1.97	45.5 ± 6.72	0.58 ± 0.10
Mean-MIL	72.5 ± 4.64	74.0 ± 4.41	42.0 ± 3.99	41.8 ± 4.31	45.4 ± 7.88	0.42 ± 0.07
ABMIL ¹⁷	81.4 ± 2.07	81.6 ± 3.62	51.0 ± 3.26	49.7 ± 4.06	52.9 ± 4.71	0.65 ± 0.04
Gate-ABMIL ¹⁷	78.9 ± 2.05	82.3 ± 3.41	54.0 ± 3.10	53.0 ± 2.78	52.7 ± 2.55	0.61 ± 0.05
CLAM-SB ¹⁹	81.9 ± 1.52	82.3 ± 3.57	54.0 ± 3.25	53.2 ± 3.30	57.0 ± 5.80	0.64 ± 0.06
CLAM-MB ¹⁹	81.7 ± 3.08	84.8 ± 4.11	57.6 ± 2.34	56.9 ± 2.07	59.0 ± 3.74	0.61 ± 0.09
DSMIL ²⁸	77.1 ± 3.38	78.9 ± 3.28	49.6 ± 2.83	49.0 ± 2.75	51.2 ± 1.73	0.57 ± 0.07
TransMIL ¹⁸	79.7 ± 1.78	83.9 ± 2.10	50.8 ± 4.61	47.1 ± 5.16	46.7 ± 7.02	0.63 ± 0.03
DTFD ²⁹	80.4 ± 1.10	78.5 ± 2.96	49.3 ± 2.60	46.4 ± 3.72	47.4 ± 7.18	0.63 ± 0.03
AMD-MIL ²⁷	81.7 ± 0.72	83.0 ± 2.83	53.1 ± 3.69	51.6 ± 3.35	55.1 ± 3.60	0.65 ± 0.04
WiKG ³⁰	80.8 ± 1.34	83.2 ± 2.79	51.6 ± 2.55	50.1 ± 5.04	51.0 ± 8.07	0.62 ± 0.03
FR-MIL ³¹	79.2 ± 3.24	83.1 ± 2.03	54.5 ± 3.56	54.5 ± 1.93	57.4 ± 4.86	0.57 ± 0.06

Table 4. Benchmark results on Camelyon⁺ dataset of the image-text contrastive pre-trained domain.

Methods	Acc (%)	AUC (%)	F1 (%)	Recall (%)	Precision (%)	Kappa
PLIP ⁵ (WSIs pre-trained)						
Max-MIL	79.4 ± 2.49	78.2 ± 3.44	43.9 ± 1.87	47.3 ± 2.13	41.2 ± 2.01	0.61 ± 0.03
Mean-MIL	73.4 ± 6.31	75.4 ± 5.08	43.7 ± 2.48	43.6 ± 3.44	48.9 ± 3.82	0.50 ± 0.05
ABMIL ¹⁷	81.8 ± 1.94	85.1 ± 4.15	53.1 ± 5.62	54.3 ± 4.08	55.0 ± 5.96	0.66 ± 0.03
Gate-ABMIL ¹⁷	82.4 ± 0.98	84.5 ± 3.91	53.4 ± 1.57	54.7 ± 2.14	54.9 ± 1.68	0.67 ± 0.04
CLAM-SB ¹⁹	81.9 ± 1.81	84.7 ± 4.43	52.0 ± 6.23	53.8 ± 4.15	51.8 ± 8.51	0.65 ± 0.04
CLAM-MB ¹⁹	83.9 ± 0.78	87.2 ± 2.20	59.8 ± 3.83	60.4 ± 4.02	60.9 ± 3.33	0.67 ± 0.04
DSMIL ²⁸	81.9 ± 2.78	84.8 ± 3.58	54.3 ± 3.03	54.2 ± 2.74	56.1 ± 4.73	0.65 ± 0.02
TransMIL ¹⁸	81.9 ± 1.57	86.3 ± 3.01	51.5 ± 7.23	54.1 ± 5.52	55.4 ± 10.71	0.65 ± 0.04
DTFD ²⁹	81.3 ± 2.22	84.2 ± 4.23	48.5 ± 4.74	51.4 ± 3.52	49.6 ± 6.55	0.66 ± 0.03
AMD-MIL ²⁷	84.9 ± 1.45	88.1 ± 2.90	57.7 ± 5.05	59.1 ± 4.34	58.9 ± 1.83	0.69 ± 0.03
WiKG ³⁰	82.3 ± 2.34	86.5 ± 4.16	57.8 ± 3.53	58.1 ± 3.31	59.4 ± 3.46	0.61 ± 0.08
FR-MIL ³¹	84.6 ± 0.99	88.2 ± 3.33	61.7 ± 5.41	62.1 ± 5.62	63.9 ± 7.14	0.67 ± 0.05
CONCH ⁹ (WSIs pre-trained)						
Max-MIL	83.8 ± 3.65	83.8 ± 5.93	52.8 ± 8.29	54.0 ± 6.86	52.8 ± 10.19	0.66 ± 0.06
Mean-MIL	77.9 ± 2.86	78.3 ± 4.54	44.8 ± 2.23	45.7 ± 2.65	46.3 ± 3.95	0.56 ± 0.04
ABMIL ¹⁷	81.8 ± 1.94	85.1 ± 4.15	53.1 ± 5.62	54.3 ± 4.08	55.0 ± 5.96	0.66 ± 0.03
Gate-ABMIL ¹⁷	85.7 ± 1.62	90.8 ± 4.57	60.4 ± 3.07	61.4 ± 3.02	63.0 ± 3.83	0.70 ± 0.06
CLAM-SB ¹⁹	86.6 ± 2.03	90.5 ± 4.97	60.9 ± 1.23	61.8 ± 2.12	64.6 ± 8.59	0.72 ± 0.04
CLAM-MB ¹⁹	88.0 ± 1.95	91.1 ± 5.02	65.1 ± 2.62	66.6 ± 2.78	66.2 ± 6.34	0.73 ± 0.06
DSMIL ²⁸	86.8 ± 1.98	88.3 ± 4.21	61.2 ± 1.66	61.5 ± 1.02	61.8 ± 3.03	0.70 ± 0.02
TransMIL ¹⁸	84.7 ± 3.80	91.6 ± 2.73	60.9 ± 3.13	62.6 ± 3.43	64.8 ± 13.42	0.71 ± 0.04
DTFD ²⁹	86.3 ± 2.68	89.7 ± 4.73	59.9 ± 2.14	61.0 ± 2.00	59.7 ± 3.39	0.72 ± 0.05
AMD-MIL ²⁷	84.1 ± 3.30	93.0 ± 3.21	64.3 ± 6.73	66.9 ± 8.02	66.0 ± 5.91	0.62 ± 0.17
WiKG ³⁰	86.2 ± 2.71	91.1 ± 4.71	63.8 ± 4.29	65.0 ± 4.28	67.5 ± 12.20	0.73 ± 0.03
FR-MIL ³¹	87.3 ± 2.62	92.3 ± 3.16	62.7 ± 3.90	63.7 ± 5.00	63.1 ± 2.65	0.70 ± 0.07

Table 5. Benchmark results on Camelyon⁺ dataset of the WSIs vision pre-trained domain.

Methods	Acc (%)	AUC (%)	F1 (%)	Recall (%)	Precision (%)	Kappa
UNI ⁶ (WSIs pre-trained)						
Max-MIL	81.1 ± 3.77	82.1 ± 5.87	50.1 ± 7.48	52.1 ± 7.05	50.1 ± 7.47	0.63 ± 0.06
Mean-MIL	74.1 ± 4.15	77.8 ± 3.53	43.5 ± 4.51	44.4 ± 3.81	43.8 ± 5.30	0.49 ± 0.08
ABMIL ¹⁷	84.6 ± 2.28	90.6 ± 2.94	59.6 ± 2.12	60.2 ± 1.62	60.4 ± 2.97	0.69 ± 0.06
Gate-ABMIL ¹⁷	84.1 ± 3.13	90.8 ± 1.01	59.7 ± 4.00	60.3 ± 3.41	63.0 ± 5.87	0.70 ± 0.04
CLAM-SB ¹⁹	83.5 ± 3.41	90.8 ± 3.82	56.4 ± 3.59	57.5 ± 2.91	56.8 ± 4.38	0.68 ± 0.03
CLAM-MB ¹⁹	88.0 ± 1.93	93.3 ± 3.40	66.6 ± 5.70	67.1 ± 6.87	70.2 ± 5.74	0.75 ± 0.04
DSMIL ²⁸	83.0 ± 3.76	87.6 ± 3.01	57.7 ± 5.76	56.7 ± 5.76	64.7 ± 13.70	0.65 ± 0.05
TransMIL ¹⁸	85.9 ± 2.32	91.9 ± 2.59	60.0 ± 10.56	62.0 ± 9.04	66.8 ± 13.03	0.72 ± 0.03
DTFD ²⁹	84.4 ± 2.97	90.4 ± 2.93	58.6 ± 4.08	59.6 ± 2.76	60.0 ± 7.16	0.72 ± 0.05
AMD-MIL ²⁷	85.3 ± 1.76	92.4 ± 1.19	60.5 ± 6.29	61.4 ± 6.37	61.7 ± 6.59	0.72 ± 0.03
WiKG ³⁰	85.6 ± 3.36	91.7 ± 2.31	62.9 ± 3.13	64.3 ± 2.39	64.2 ± 8.35	0.73 ± 0.03
FR-MIL ³¹	85.2 ± 2.81	93.0 ± 2.20	65.2 ± 4.46	64.9 ± 5.57	70.9 ± 9.53	0.69 ± 0.05
Gigapath ⁷ (WSIs pre-trained)						
Max-MIL	81.4 ± 6.62	86.6 ± 6.96	55.4 ± 5.93	54.6 ± 5.35	54.9 ± 5.53	0.65 ± 0.11
Mean-MIL	77.4 ± 3.20	79.1 ± 3.17	46.3 ± 4.24	46.3 ± 4.61	53.6 ± 9.24	0.53 ± 0.09
ABMIL ¹⁷	79.2 ± 2.43	92.1 ± 0.27	65.7 ± 6.11	58.1 ± 5.31	58.6 ± 0.99	0.68 ± 0.03
Gate-ABMIL ¹⁷	84.9 ± 3.00	89.7 ± 3.41	59.6 ± 1.61	58.7 ± 2.70	59.5 ± 4.52	0.69 ± 0.04
CLAM-SB ¹⁹	85.4 ± 2.93	91.2 ± 2.47	60.8 ± 3.78	59.8 ± 3.56	63.7 ± 8.90	0.72 ± 0.03
CLAM-MB ¹⁹	86.7 ± 3.01	92.1 ± 2.88	69.1 ± 8.13	66.7 ± 5.36	67.0 ± 3.40	0.70 ± 0.07
DSMIL ²⁸	86.5 ± 3.12	89.7 ± 4.70	62.1 ± 4.48	62.3 ± 2.86	64.2 ± 2.46	0.68 ± 0.06
TransMIL ¹⁸	88.2 ± 2.77	92.8 ± 2.44	67.4 ± 3.54	66.9 ± 2.68	75.5 ± 11.95	0.73 ± 0.07
DTFD ²⁹	83.7 ± 2.33	89.4 ± 4.64	59.4 ± 3.78	58.0 ± 4.24	61.3 ± 3.57	0.68 ± 0.07
AMD-MIL ²⁷	87.3 ± 1.92	92.6 ± 3.11	65.8 ± 4.68	64.6 ± 4.28	64.6 ± 4.42	0.72 ± 0.05
WiKG ³⁰	85.0 ± 3.89	91.3 ± 2.93	59.5 ± 5.13	59.4 ± 6.88	68.0 ± 16.12	0.72 ± 0.06
FR-MIL ³¹	86.2 ± 2.01	90.7 ± 3.11	63.2 ± 3.54	63.8 ± 2.40	75.7 ± 10.20	0.71 ± 0.06